

Strain analysis in ferritic filler weldment by using the modified Williamson-Hall method

Mohammad Dani ^{a,*}, Aziz Khan Jahja ^a, Parikin ^a, Andon Insani ^a, Riza Iskandar ^b

^a Center for Science and Technology of Advanced Materials, BATAN Kawasan Puspipstek, Serpong Tangerang 15314, Indonesia

^b Central Facility for Electron Microscopy (GFE), RWTH Aachen University, Ahornstr. 55, D-52074 Aachen, Germany

* Corresponding author: mdani@batan.go.id

Article history

Received 3 October 2017

Accepted 28 November 2017

Abstract

A strain analysis study of the Fe-Cr-Ni based low carbon steel for welding application prepared by a thermal-induction furnace were performed using a modified Williamson-Hall (MHW) method. Three different models, uniform deformation (UDM), the uniform deformation stress (UDSM), and the the uniform deformation energy density (UEDM) models. The optimal results showed by calculation result using UDM method indicate that uniform deformation was present on analyzed material. Based on UDM method, the welded material contains smaller grain size than the based materials. The calculated of average microstrain values of 7.6351×10^{-4} and -9.21×10^{-4} for based and welded materials respectively suggest different strain phenomena occurs during welding processes. Microstructure analysis by means of transmission electron microscopy reveal that based material consist of grains in 50-100 nm sizes and with planar defects are also detected.

Keywords: Nano-structured materials, chemical synthesis, crystal structure, TEM, W-H analysis

© 2017 Penerbit UTM Press. All rights reserved

INTRODUCTION

Fe-Cr-Ni based low carbon steels are still the subject of many research activities. They exhibit lower strength but higher ductility/toughness. Typical application may include heat exchanger appliances, automotive and architectural trim (i.e. decorative purposes). Some of research activities are aimed to understand the mechanical and physical properties of non-standard low carbon steels, in which the composition of the steel-alloys does not follow the preset AISI standards [1]. This type of sample composition is also not available before in the free market [2,3,4]. Therefore, these samples and their properties represent a state of the art new development in materials technology especially for welding applications.

As welding induces a large amount of strain in the bulk samples [5], systematically study for both based and weld materials need to be performed. Lattice strains are commonly encountered in welded components, because of lattice deformation [6]. This is caused by several factors, such as the thermal expansion effects of welding, the pre-welding fabrication and post-welding treatment cause the strain state to arise in the welded plates and bars. And these various influences may also be the cause of disintegration of the material's structural integrity, because of the ensuing reduced fatigue life or increased susceptibility to environmentally assisted failure mechanisms.[7,8].

One of powerful technique to analysis strain formation of weld materials is by means of Neutron profile analysis. [8]. One of method to analysis strain formation is by using Williamson-Hall (W-H) analysis. This method is a simplified integral breadth method where both size-induced and strain-induced broadening are deconvoluted by considering the peak width as a function of 2θ [9]. In the present study, W-H analysis is employed for estimating crystallite size and lattice strain.

In this present work three modified forms of W-H uniform deformation (UDM), uniform deformation stress (UDSM) and uniform

deformation energy density models (UEDM) were applied [10]. To strengthen the strain analysis, microstructure analysis by means of transmission electron microscopy technique is also presented.

THEORY

When a sample is subjected to homogenous strain, the peak's angular position will shift to either lower or higher 2θ values depending on whether a *yield*- or a *tensile*-strain is being applied on the sample. On the other hand, an *inhomogeneous* strain field will cause besides an angular shift also a broadening in the intensity profile. Experimentally, heating and cooling a metallic specimen will induce lattice strain in the specimen. The shift in peak-position is tied to the average strain in the crystal's direction. The peak broadening reveals information on the inhomogeneous strain-field distribution fluctuation [5]. The average lattice strain in the crystal direction $[hkl]$, is expressed by:

$$\varepsilon_{hkl} = \frac{d - d_0}{d_0} \quad (1)$$

Here d_0 and d are stress-free and stress-induced lattice-distance respectively. In table 3, the ε_{hkl} and d_{hkl} values for each treatment phase are presented and compared. The profile broadening induced by inhomogeneous strain-field e^2_{hkl} is expressed as:

$$\beta_{hkl}^2 = \beta_0^2 + 32 \ln 2 \varepsilon^2 (\tan \theta)^2 \quad (2)$$

β_{hkl}^2 is the FWHM of peak broadening and β_0^2 is the angular dependent instrument resolution, given by the Cagliotti expression [6,7] as follows:

$$\beta_o^2 = U_o(\tan\theta)^2 + V_o(\tan\theta) + W_o \tag{3}$$

U_o , V_o , and W_o are the three Gaussian FWHM parameters. Using the RIETAN-refined values of U_o , V_o , and W_o presented in table 4. The significance of the broadening of peaks evidences grain refinement along with the large strain associated with the powder. The instrumental broadening (β_{hkl}) was corrected, corresponding to each diffraction peak of 73Fe24Cr2Si0.8Mn0.1Ni material using the relation:

$$\beta_{hkl} = (\beta_{hkl,measured}^2 - \beta_{hkl,instrumental}^2)^{1/2} \tag{4}$$

When crystals' size is less than 1000 Å (0.1 μm), crystals of this size will contribute to a broadening of the Debye rings, the extent of the broadening β_{hkl} and the average nanocrystalline size is given as the Debye-Scherrer's formula;

$$D = \frac{K\lambda}{\beta_{hkl}} \frac{1}{\cos\theta} \tag{5}$$

where D = crystalline size, K = shape factor (0.9), and λ = wavelength of neutron radiation 1.8223 Å. Assuming that the particle size and strain contributions to line broadening are independent to each other and both have a Cauchy-like profile, the observed line breadth is simply the sum of Equations 2 and 3.

$$\beta_{hkl} = \frac{K\lambda}{D\cos\theta} + 4\epsilon\tan\theta \tag{6}$$

Size and strain in a polycrystalline sample could be separated with the Williamson-Hall method. Williamson-Hall method is used to determine the crystallite size and microstrain in order to make comparison with the results obtained from the whole pattern refinements. It was suggested that the broadening due to size and microstrain can be expressed as [5],

$$\beta_{hkl}\cos\theta = \frac{K\lambda}{D} + 4\epsilon\sin\theta \tag{7}$$

where D is the crystallite diameter size (Å) and ϵ is the average maximum micro strain. Plotting $\beta_{hkl} \cos \theta$ versus $\sin \theta$, will result in a straight line. In this case, the microstrain is obtained from the slope of the regression line and the intercept with the vertical axis is related to the value of the inverse of the size (nanosize) of the particles. In this case, some of the mechanical effects such as the energy density and the stress of the uniform deformation were taken also considered; Assumption that the Young modulus of the crystal is anisotropic is more in line with reality [9]. In the generalized Hook's law the stress is linearly proportional to the and strain, and in this case the constant of proportionality is the modulus of elasticity or Young modulus, denoted by E . Then the Williamson-Hall equation is modified by substituting the value of ϵ in Equation 7; one obtain

$$\beta_{hkl}\cos\theta = \frac{K\lambda}{D} + 4\sin\theta \frac{\sigma}{E_{hkl}} \tag{8}$$

E_{hkl} is Young's modulus in the direction perpendicular to the set of the crystal lattice plane (hkl).

From the slope of the linear plot between $4\sin\theta/E_{hkl}$ and β_{hkl} , the uniform stress - and from the intercept the crystallite size D can be calculated. The strain can be measured if E_{hkl} of cubic 73Fe24Cr2Si0.8Mn0.1Ni is known. For samples with a cubic crystal phase, the relation between the Young's modulus E_{hkl} to their elastic compliances S_{ij} is stated as [5,7];

$$\frac{1}{S_{11} - 2S_{44}} \frac{1}{hkl} \tag{9}$$

With the degree of anisotropy given as,

$$A_{hkl} = \frac{h^2k^2 + h^2l^2 + l^2k^2}{h^2 + k^2 + l^2} \tag{10}$$

and

$$S = 1/2(S_{11} - S_{12} - S_{44}) \tag{11}$$

The values of the S_{11} , S_{12} , and S_{44} elastic compliances of Fe iron are 0.80×10^{-11} , -0.28×10^{-11} and $0.86 \times 10^{-11} \text{ Pa}^{-1}$, respectively [5]. According to Hooke's law, the energy density e (energy per unit volume) as a function of strain is $e = \epsilon^2 E_{hkl}/2$. Therefore the uniform deformation energy density (UDEM) can be calculated from the slope of the linear graph in the $\beta_{hkl} \cos\theta$ vs. $4\sin\theta (2/E_{hkl})^{1/2}$ plot, by first modifying Equation 6 to the form,

$$\beta_{hkl}\cos\theta = \frac{K\lambda}{L} + 4\sin\theta \sqrt{\frac{2e}{E_{hkl}}} \tag{12}$$

where e is the energy density (energy per unit volume). The lattice strain can be calculated by knowing the Young moduli E_{hkl} values of the sample

MATERIALS AND METHODS

Materials

The low carbon stainless steel consists primarily of base materials such as of ferro scrap, ferro-chrome, ferro-manganese, ferro-silicon; all of them are in granular form and are minerals products obtained from domestic mines. Details of the chemical composition of both base and filler materials are listed in Table 1.

Table 1. The Chemical composition of 73Fe24Cr2Si0.8Mn 0.1Ni low carbon steel.

Element	%wt.
Fe	72.97
Ni	0.12
Cr	23.71
Mn	0.82
Si	2.02
C	0.26
Al	0.01
S	0.01
P	0.02
V	0.06
Ti	0.01
Sn	0.01
Nb	0.01

The base metal is the 73Fe24Cr2Si0.8Mn0.1Ni (in %wt.) stainless steel and the filler metal was also ferritic type stainless steel. The samples, as seen in Figure 1, have dimension of 200 x 10 x 5 mm³, and designated for base and filler-welded at 350 ° C respectively. The sample preparation follows the common standard metallographic procedure [12]. Welding processes were performed using the manual Gas Tungsten Arc Welding (GTAW) technique. Details of welding parameters are given in Table 2.

For the neutron diffraction measurement and pre-welding preparation the ferritic samples are prepared by mechanical method into bulk shape of approximately 1.5 x 1.5 cm² in wide-thick and 60.0 cm in length and the surface was mechanically grinded into flat surface and polished-cleaning to remove any surface oxides and contaminants.

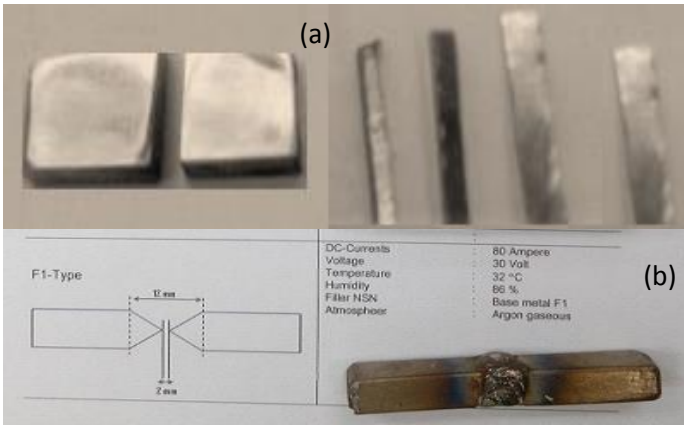


Fig. 1 (a) The Fe-Cr-Ni base and the filler welded materials, (b) Welding schema and (60x15x15 mm³) dimension of weld specimens used in neutron diffraction measurements.

Table 2. TIG-weld parameters for 73Fe24Cr2Si0.8Mn0.1Ni alloy sample.

TIG-weld Parameters	
Welding Type	: GTAW
Dimension	: 50 x 15 x 15 mm ³
Atmosphere	: Argon
Current	: 80 A
Voltage	: 30 V
Speed	: 60 mm/min

Apparatus and Methods

Strain and strain analysis were performed by means neutron powder diffraction techniques. High resolution powder diffractometer (HRPD) spectrometer from located at Neutron Scattering Laboratory attached to the G.A.S. Siwabessy Research Reactor at BATAN in Serpong was used. The neutron wavelength of $\lambda = 1.8223 \text{ \AA}$ was determined from calibration measurements of four diffraction peaks from a silicon standard powder sample, the step counting mode with an incremental step of 0.05° was used. The focused ion beam (FIB) technique has been employed to prepare lamella for transmission electron microscopy (TEM) analysis. A single beam Strata 205 from FEI was used to prepare the lamella [11]. The TEM analysis were performed on Zeiss Libra 200 FE, a Schottky field emission TEM operates at 200 keV. The microscope equipped within column corrected omega filter, a high angle angular dark field (HAADF) and energy dispersive spectrometer (EDS) detectors from fischione and bruker respectively

RESULTS AND DISCUSSION

Neutron diffraction analysis

The Neutron Diffraction pattern of the base material as shown in Figure 2 is having a cubic structure with no extra diffraction peaks belongs to secondary phase. The peaks' intensity is sharp and narrow, confirming that the sample is of high quality with good crystallinity and fine grain size. Using HRPD data, lattice parameters were refined and the results presented in Table 3.

Table 3. Refined neutron diffraction structural Parameters of Fe-Cr-Ni alloy(base and welded with filler condition).

Phase ^{s)} α -Fe	Lattice parameter a (Å) ^{r)}	R_{wp} (%)	R_p (%)	R_e (%)
Condition				
base	2.8745(4)	126.0	74.43	27.05
welded with filler	2.8689(3)	90.80	47.80	19.60

^{s)}SG. Fm3m (vol. I-225) ;1601 data points, 4 reflections (110), (200), (211) and (220)

^{r)} The number inside parentheses indicates the uncertainty of the last significant digit

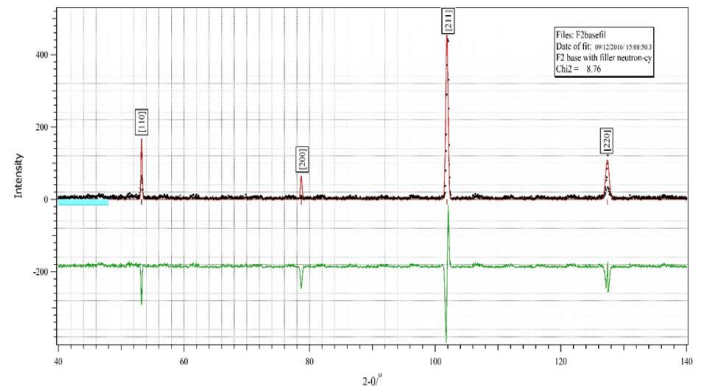


Fig. 2 HRPD neutron diffraction pattern of 73Fe24Cr2Si0.8Mn0.1Ni base material.

The neutron diffraction pattern of the filler-welded material (Figure 3) shows additional peaks from secondary phase as addition to the matrix which could form filler material in the weldment zone.

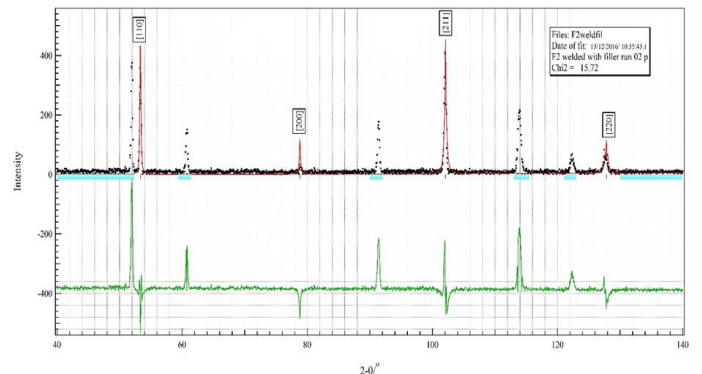


Fig. 3 HRPD neutron diffraction pattern measured in weldment zone of 73Fe24Cr2Si0.8Mn0.1Ni filler-welded sample.

Further analysis using Rietveld refinemet procedures were applied by excluding additional peaks from secondary phase. The results are presented in Table 1. The refinement results are also used to calculate the strain-free and strain-induced lattice-distances, d_o and d , which are used in the calculation of e_{hkl} as presented in Table 4.

Table 4 Comparison of average lattice strain e_{hkl} and d_{hkl} values for the base and filler-welded samples^{s)} and Comparison of Relative Intensity of Major Peaks and FWHM.

[hkl]	Base	Filler-welded	
	$d_{hkl,0}$ (Å)	d_{hkl} (Å)	$e_{hkl} \times 10^{-3}$
[110]	2.032598(4)	2.028566(4)	1.9837(5)
[200]	1.437264(3)	1.424413(2)	1.9836(2)
[211]	1.173521(2)	1.171193(2)	1.9838(2)
[220]	1.016299(2)	1.014283(1)	1.9836(7)
		Average	1.9836(3)

^{s)} The number inside parentheses indicates the uncertainty of the last significant digit.

The three Gaussian FWHM (β_{hkl}) parameters, U_o , V_o , and W_o , for both the base and the filler-welded 73Fe24Cr2Si0.8Mn 0.1Ni samples, are shown in Table 5. These parameters are used to calculate the FWHM (β_{hkl}) values using equations (2) and (3) as presented in Table 6.

Table 5. Gaussian FWHM (β_{hkl}) parameters U_o , V_o W_o .

Samples	U_o	V_o	W_o
Base	0.104123(3)	-0.0104910(5)	0.035367(3)
Welded with filler	0.008875(4)	-0.0076180(1)	0.050610(0)

Table 6. FWHM (β_{hkl}) from Rietveld refinement results of base- and filler-welded 73Fe24Cr2Si0.8Mn0.1Ni sample.

[hkl]	Relative I_o (counts) base	fwhm (β_{hkl}) (rad) base $\times 10^{-3}$	Relative I_o (counts) welded with filler	fwhm (β_{hkl}) (rad) Welded with filler $\times 10^{-3}$
[110]	37000	3.7441	65854	4.1409
[200]	10300	3.6994	12200	5.4283
[211]	100000	3.6824	100000	7.4761
[220]	20200	3.7776	35350	1.1586

Strain analysis using the modified Williamson-Hall plot

In Table 7 below the Young moduli E_{hkl} calculated using equations (9-11) are presented.

Table 7. The Young moduli E_{hkl} calculated using equations (9-11).

hkl	(110)	(200)	(211)	(220)
E_{hkl} (GPa)	144.93	125.00	212.77	277.8

Using equations (1-11) the various mechanical properties of 73Fe24Cr2Si0.8Mn0.1Ni nanoparticles such as mean particle size obtained from direct TEM measurements and from neutron diffraction (HRPD) peak broadening and the strain associated with the base and filler-welded 73Fe24Cr2Si0.8Mn0.1Ni samples at 450°C due to lattice deformation could be calculated and plotted according to different Williamson-Hall modified models, namely, uniform deformation model (UDM), the uniform deformation stress model (UDSM), and the uniform deformation energy density model (UEDM).

The Williamson-Hall plot using the UDM method for the base and the filler-welded 73Fe24Cr2Si0.8Mn0.1Ni sample is presented in Figure 4 and Figure 5 below.

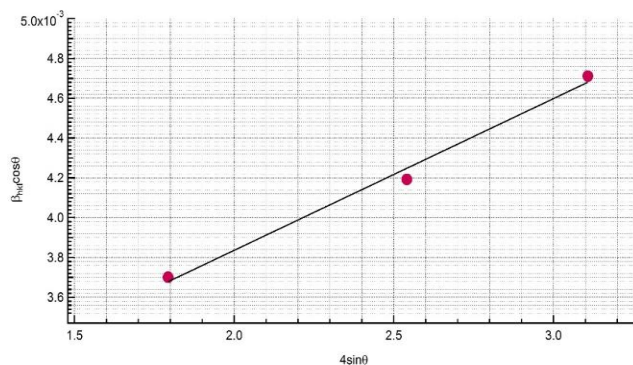


Figure 4. The modified Williamson-Hall plot using the UDM model obtained by using profile fitting of the neutron diffraction pattern of a base 73Fe24Cr2Si0.8Mn0.1Ni bar. The straight regression lines are obtained by least-square method.

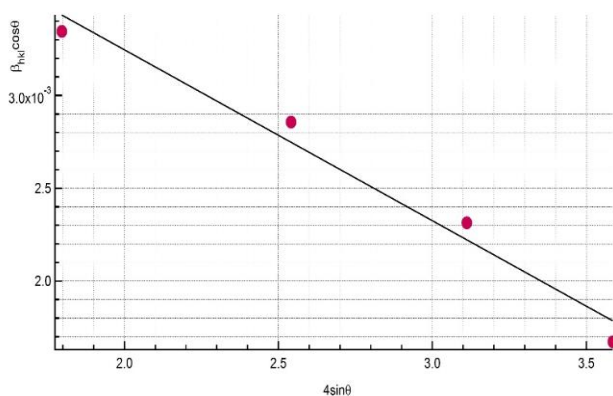


Figure 5. The modified Williamson-Hall plot using the UDM model obtained by using profile fitting of the neutron diffraction pattern in the HAZ region of a filler-welded 73Fe24Cr2Si0.8Mn0.1Ni bar. The straight regression lines are obtained by least-square method.

The Williamson-Hall plot using the UDSM method for the base and the filler-welded 73Fe24Cr2Si0.8Mn0.1Ni sample is presented in Figure 6 and Figure 7 below.

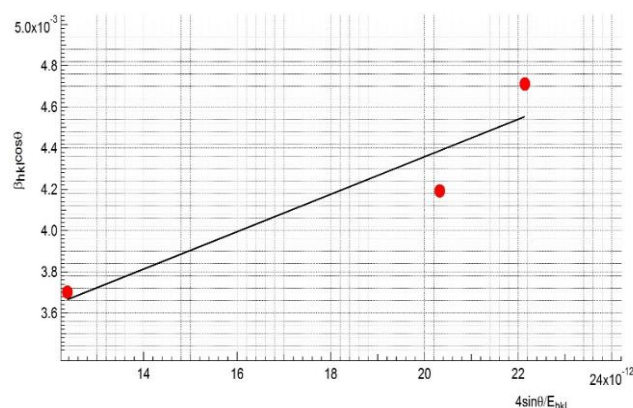


Figure 6. The modified Williamson-Hall plot using the UDSM model obtained by using profile fitting of the neutron diffraction pattern of a base 73Fe24Cr2Si0.8Mn0.1Ni bar. The straight regression lines are obtained by least-square method.

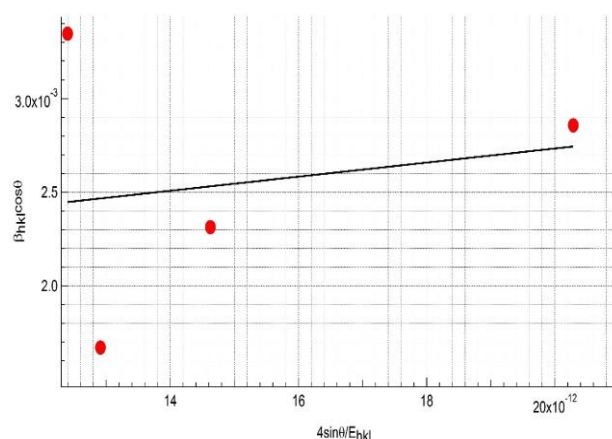


Figure 7. The modified Williamson-Hall plot using the UDSM model obtained by using profile fitting of the neutron diffraction pattern in the HAZ region of a filler-welded 73Fe24Cr2Si0.8Mn0.1Ni bar. The straight regression lines are obtained by least-square method.

The Williamson-Hall plot using the UEDM method for the base and the filler-welded 73Fe24Cr2Si0.8Mn0.1Ni sample is presented in Figure 8 and Figure 9 below.

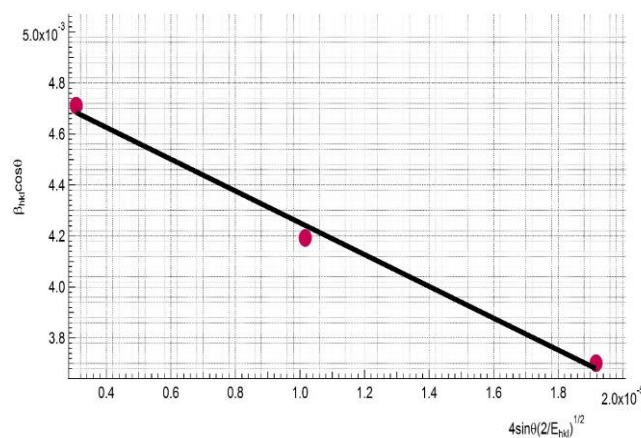


Figure 8. The modified Williamson-Hall plot using the UEDM model obtained by using profile fitting of the neutron diffraction pattern of a base 73Fe24Cr2Si0.8Mn0.1Ni bar. The straight regression lines are obtained by least-square method.

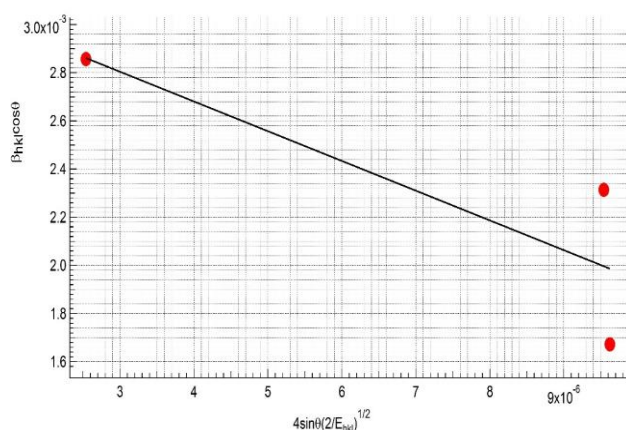


Figure 9. Williamson-Hall plot using the UEDM plot obtained by using profile fitting of the neutron diffraction pattern in the HAZ region of a filler-welded 73Fe24Cr2Si0.8Mn0.1Ni bar. The straight regression lines are obtained by least-square method.

By comparing the values of average crystallite size obtained from UDM, USDM, and UEDM, it was found that the values are not at all similar, implying that the inclusion of strain in various forms has a very large effect on the average crystallite size 73Fe24Cr2Si0.8Mn0.1Ni alloy particles [6,12]. For the base 73Fe24Cr2Si0.8Mn0.1Ni sample, the largest value of crystallite size is found from the UDM method (71.04 nm), and decreases for the USDM and the UEDM method, which is 64.53 nm and 33.64 nm respectively. In the weldment region of the filler-welded sample, all three methods predict that the crystallite size would be altered as a result of welding. The UDM method predicts that the crystallite size *D* would decrease (32.24 nm), whereas both the USDM and the UEDM method predict that *D* would increase to 82.67 nm and 51.69 nm respectively, so there is a considerable change in the grain size after welding. But these results are consistent with the premise that only grains with sizes $\leq 0.1 \mu\text{m}$ would contribute to profile broadening. However, the energy density value ϵ could not be evaluated from the UEDM method since the slope of the linear plot is negative, and therefore has no real physical meaning. Therefore this method may not be valid in this case of massive bulk materials.

Table 8. The Geometric Parameters of 73Fe24Cr2Si0.8Mn0.1Ni steel obtained form modified Williamson-Hall method.

Method	UDM		USDM			UEDM		
	D (nm)	ϵ	D (nm)	Σ (MPa)	ϵ	D (nm)	ϵ (kJm ⁻³)	ϵ
Base	71.04	7.6351×10^{-4}	64.53	90.83	4.9364×10^4	33.64	-	-
Filler-welded	32.24	-9.21×10^{-4}	82.67	37.48	2.037×10^{-4}	51.69	-	-

Microstructure analysis from transmission electron microscopy data

Figure 10 shows Bright-Field TEM image of Fe-Cr-Ni sample taken from area close to the surface. The elemental analysis from other report at reference of the work of Parikin et.al revealed the large of Al₂O₃ grain formed inside the matrix. A thin layer of SiO₂ formed at the matrix-alumina interface. TEM Bright-field image shows high deformations and defects presence on the matrix (Figure 10.a). These defects are also found at oxide – precipitates interface. EDS-analysis identified the precipitate as Cr-carbide precipitate [12].

It was observed that two layers of dense Al₂O₃ scale with a total thickness of 200 to 300 nm. Therefore, in this case, lattice strain in the 73Fe24Cr2Si0.8Mn0.1Ni sample bulk could well be caused by the presence of an excess volume of dislocation grain boundaries [8]. The dimension of the grains as is evident from the TEM images somehow matches the order of magnitude of the size of the crystallite *D* presented in Table 8, which is bigger than 100 nm.

The presence of microcracks (overlapping layers) on the precipitates was also observed in the surface. As can be seen on Figure 10.b, the overlapping layers developed on interface of chromia precipitate causing the strains in materials. Additional magnification image of selected area shows that overlapping layers also present dislocation at the Al₂O₃-matrix interface.

Higher magnification images of selected areas (marked by rectangular A1 and A2) revealed high deformations and defects presence on the matrix as seen in figure 10(b) and (c) respectively. On figure 10 (b), diffraction contrast, which indicates different crystal orientation, appears also in layer forms at the alumina interface. Moreover, SiO₂ thin layer approximately 100 nm thick, which was detected by EDX analysis, appears as amorphous layer. Higher magnification image of area 2, where a precipitate formed, probably Cr-C based on EDX analysis, shows similar condition with area 1. On contrast with the matrix, diffraction contrast revealed that the precipitates is almost free from defects. Highly defects and dislocation

grain boundaries formed in the matrix could be the cause of the lattice strain in the 73Fe24Cr2Si0.8Mn0.1Ni sample bulk [8].

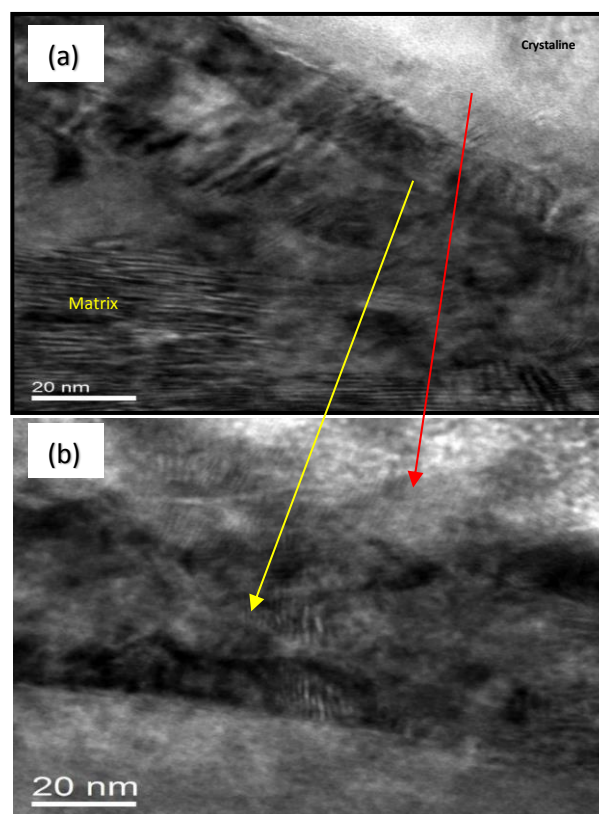


Figure 10. A higher magnification of TEM Bright-Field image on the 73Fe24Cr2Si0.8Mn0.1Ni base sample to show deformation and defects.

CONCLUSION

A new low carbon sample $73\text{Fe}24\text{Cr}2\text{Si}0.8\text{Mn}0.1\text{Ni}$ was synthesized and prepared as base and welded specimens. Both BF TEM analysis and High-resolution powder neutron diffraction analysis are carried out on these samples. Based upon the deep and broad intensity Rietveld analysis of the neutron diffraction experimental data presented, it is observed that the new Low Carbon alloy $73\text{Fe}24\text{Cr}2\text{Si}0.8\text{Mn}0.1\text{Ni}$ is a typical example of the dependence of average lattice strain e_{hkl} on a diffraction plane $[hkl]$ caused by an elastic anisotropy of the crystal. The average value of $4.396(3) \times 10^{-4}$ for the average lattice strain (microstrain) e_{hkl} has been observed in the rolled $73\text{Fe}24\text{Cr}2\text{Si}0.8\text{Mn}0.1\text{Ni}$ sample. Higher resolution analysis by means TEM revealed the presence of high defects formation on matrix which could explain the lattice strain measurement results that is bigger than 100 nm. On the other hand, an angular shift and a broadening in the intensity profile for all diffraction planes as an evidence of an *inhomogeneous* strain field were observed in the weldment area of $73\text{Fe}24\text{Cr}2\text{Si}0.8\text{Mn}0.1\text{Ni}$ samples. Evidence of the plane dependence of the strain and microstrain necessitates that this study should be continued with neutron diffraction internal stress measurement using the DN1 Powder diffractometer.

ACKNOWLEDGEMENT

The authors would like to express his gratitude to Mr. Gunawan, head of PSTBM-BATAN, and Dr. Abu-Khalid Rivai head of BSBM-PSTBM and Dr. Eng. Iwan Sumirat head of BTBN-PSTBM for their continuing valuable support for this research project in the fiscal year of 2016 and the conducive research climate, which facilitates both the continuation and the finishing of this program at PSTBM-BATAN. The authors also wish to thank Mr. Herry Mugiraharjo from BTBN-PSTBM for the neutron HRPD measurement

REFERENCES

- [1] B. A. Pint, K. A. Terrani, M. P. Brady, T. Cheng, J. R. Keiser. (2013). High temperature oxidation of fuel cladding candidate materials in steam-hydrogen environments. *J. Nucl. Mater.*, 440(1), 420–427.
- [2] A. K. Jahja (2010). Ferritic stainless steel synthesis from mining materials, In Evvy Kartini, B. V. R. Chowdari, Aziz Khan Jahja, S. Selvasekarapandian, Tutun Nugraha, Junichiro Mizusaki, Sudaryanto, S. J. Kennedy, Heri Jodi. *Proceedings of the ICMST 2010*. Paper presented at International Conference on Materials Science & Technology, Serpong (61-68). Serpong: PTBIN-BATAN & MRS-INA.
- [3] T. Darwinto and A.K. Jahja. (2010). Microstructure and crystal structure analysis of F1 ferritic steel. *Indonesian Journal of Materials Science*, 11 (3), 202-206.
- [4] K. A. Terrani, B. A. Pint, Y. -J. Kim, K. A. Unocic, Y. Yang, C. M. Silva, H. M. Meyer, R. B. Rebak. (2016). Uniform corrosion of FeCrAl alloys in LWR coolant environments. *J. Nucl. Mat.*, 479, 36-47.
- [5] Noyan, Ismail C., Cohen, Jerome B. (1987). *Residual Stress: Measurement by Diffraction and Interpretation*, Springer Verlag, New York.
- [6] C. -H. Cho, S. -G. Lee, T. -H. Lee, J. Lee. (2013). Fabrication and electrical properties of $\text{YBa}_2\text{Cu}_3\text{O}_{7-x}$ thin film prepared by sol-gel method for uncooled infrared detectors. *J. Ceram. Process. Res.*, 14(3), 436-439.
- [7] S. I. Talabi, O. B. Owolabi, J. A. Adebisi, T. Yahaya. (2014). *Adv. Prod. Eng. Management (APEM)*, 9(4), 181–186.
- [8] A. N. Ezeilo and G. A. Webster. (1999). Advances in neutron diffraction for engineering residual stress measurements. *Textures and Microstructures*, 33, 151-171.
- [9] F. G. Kevin, N. G. Maxim, Y. Yukinori, L. S. Lance. (2014). Deformation behavior of laser welds in high temperature oxidation resistant Fe–Cr–Al alloys for fuel cladding applications. *J. Nucl. Mat.* 454, 352-358.
- [10] V. D. Mote, Y. Purushotham, B.N. Dole. (2012). Williamson-Hall analysis in estimation of lattice strain in nanometer-sized ZnO particles. *Journal of Theoretical and Applied Physics*. Retrieved from <http://www.jtaphys.com/content/2251-7235/6/1/6>.
- [11] H. Dai, J. A. Francis, H. J. Stone, H. K. D. H. Bhadeshia, and P. J. Withers. (2008). Characterizing Phase Transformations and Their Effects on Ferritic Weld Residual Stresses with X-Rays and Neutrons. *Metall. Mater. Trans. A*, 39(13), 3070-3078.
- [12] M. Dani, P. Untoro, T. Y. S. P. Putra, Parikin, J. Mayer and A. Dimiyati. (2015). Transmission Electron Microscopy Characterization of High-Temperatur Oxidation of Fe-20Cr-5Al Alloy Prepared by Focused Ion Beam Technique. *Makara J. Technol.* 19(2), 85-89.
- [13] Parikin, M. Dani, A. K. Jahja, R. Iskandar and J. Mayer. (2017). Crystal Structure Investigation of Ferritic $73\text{Fe}24\text{Cr}2\text{Si}0.8\text{Mn}0.1\text{Ni}$ Steel for Multipurpose Structure Material Applications. *IJTech*, 8(5), 1-6.